11th International Conference on Fast Sea Transportation
FAST 2011, Honolulu, Hawaii, USA, September 2011

Dual-operating-point blade optimization for high-speed propellers

Brenden Epps, Oscar Víquez, and Chryssostomos Chryssostomidis

Sea Grant Design Lab, Massachusetts Institute of Technology, Cambridge, Massachusetts, USA

ABSTRACT

Propeller blade design for fast ships is often driven by cavitation constraints. A tradeoff exists, where larger chord lengths and section thicknesses typically improve cavitation performance but result in lower efficiency. Typically, chord lengths are optimized for the design condition (ship endurance speed), with some specified margin to prevent cavitation off-design (at maximum ship speed). Cavitation performance at the maximum speed is considered post-facto, and blade shape often needs to be modified for cavitation considerations in high-speed operation.

This paper presents an improved method for blade shape optimization. The present method simultaneously considers the cavitation performance at the endurance speed design point and a maximum speed off-design point, and blade chord lengths and thicknesses are set to prevent cavitation at both operational conditions. During the present design optimization routine, the on-design load distribution is optimized, and the off-design performance is determined, such that the chord lengths can be set to a minimum that still prevents cavitation at both the on- and off-design conditions.

A case study is presented, considering the notional design of a propeller for the U.S. Navy DDG51 destroyer-class ship. Propellers designed using standard chord/thickness optimization procedures are compared to those designed using the present procedures. Cavitation performance is compared for the two design methods.

KEY WORDS

propeller design, cavitation, blade optimization, chord length optimization, analytic bucket diagram

1.0 INTRODUCTION

We seek a deterministic approach for optimizing propeller blade chord and thickness in such a way as to maximize efficiency, provide requisite blade strength, and mitigate cavitation. For maximum efficiency, one desires zero chord lengths, since viscous losses scale with chord. However, structural considerations require finite chord and thickness, and increasing chord typically improves cavitation performance as well. So it is apparent that one can not arbitrarily choose the chord and thickness distributions but rather needs a deterministic optimization approach.

A number of design procedures exist to choose the chord and thickness distributions to prevent cavitation at a single design point, which either involve design tables (e.g. Brockett (1966)) or curve fits to these tables (e.g. Coney (1989)). However, these methods fail when multiple design points are considered. Herein, we consider the problem of optimizing loading for maximum efficiency at a ship's 20 knot *endurance speed* while optimizing the chord and thickness distributions to prevent cavitation at both the endurance speed and a 30 knot *maximum speed*. Since we aim to optimize the design at an off-design condition, the methods of Brockett (1966) and Coney (1989) do not apply, and we need a new method to optimize the blade shape to prevent cavitation.

Herein, we employ propeller lifting line theory for the design optimization and analysis (§2.0). In §2.3, we develop an analytic equation to predict the cavitation performance of each 2D blade section. In §3.0, we develop a design procedure to optimize blade loading for maximum efficiency at an endurance speed while mitigating cavitation at a maximum speed. This procedure is illustrated in §4.0 in application the DDG51 destroyer-class vessel.

2.0 THEORY

2.1 Propeller lifting-line formulation

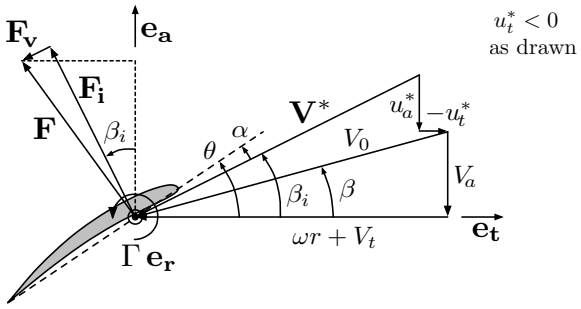

Figure 1: Propeller velocity diagram at radius r.

In *moderately-loaded* propeller lifting line theory (Lerbs, 1952; Epps, 2010b), a propeller blade is represented by a vortex line, with trailing vorticity aligned to the local flow velocity (free-stream plus induced velocity). The induced velocities are computed using a vortex lattice, with helical trailing vortex filaments shed at discrete stations along the blade. The blade is also modeled as discrete vortex panels, having 2D section properties at each radius. Loads are computed by integrating the 2D section loads over the span.

Fig. 1 illustrates the velocities and forces (per unit radius) on a 2D blade section: axial and tangential inflow velocities, V_a and V_t; axial and tangential induced velocities, u_a^* and u_t^*;

and angular velocity ω. The total resultant inflow velocity has magnitude $V^* = \sqrt{(V_a + u_a^*)^2 + (\omega r + V_t + u_t^*)^2}$ and is oriented at pitch angle β_i to the $\mathbf{e_t}$ axis. Also shown on Fig. 1 are the angle of attack, α; blade pitch angle $\theta = \alpha + \beta_i$; circulation, Γ; inviscid Kutta-Joukowski lift force, $F_i = \rho V^* \Gamma$; and viscous drag force, $F_v = \frac{1}{2}\rho (V^*)^2 C_D c$, where ρ is the fluid density, C_D is the section drag coefficient, and c is the chord.

The 3D propeller geometry is built from given 2D section profiles that are scaled and rotated according to the chord length and the design point lift coefficient and inflow angle $\{c, C_{L_e}, \beta_{i_e}\}$ such that $C_L = C_{L_I} = C_{L_e}$ and $\alpha = \alpha_I$ at the (endurance speed) design point:

$$\left\{ C_L, \alpha_I, \frac{f_0}{c} \right\} = \frac{C_{L_e}}{\widetilde{C}_{L_I}} \cdot \left\{ \widetilde{C}_{L_I}, \widetilde{\alpha}_I, \frac{\widetilde{f}_0}{c} \right\} \tag{2.1}$$

$$\theta = \alpha_I + \beta_{i_e} \tag{2.2}$$

where C_{L_I} and α_I are the ideal lift coefficient and angle of attack, and the tilde values are the given profile (Abbott and Doenhoff, 1959).

The off-design performance of a propeller is computed using the method of (Epps, 2010a). Each operating state is defined by the ship speed, V_s, rotation rate, ω, and unknown parameters $\{V^*, \alpha, C_L, \Gamma, u_a^*, u_t^*, \beta_i, \bar{u}_a^*, \bar{u}_t^*\}$. Since there are M vortex panels, there are $7M + 2M^2$ unknowns and a system of as many non-linear equations. This system is solved using a Newton solver, which drives the following residual vector to zero (for each blade section).

$$\mathbf{R} = \begin{bmatrix} V^* & - & \sqrt{(V_a + u_a^*)^2 + (\omega_m r_c + V_t + u_t^*)^2} \\ \alpha & - & (\alpha_I + \beta_{i_e} - \beta_i) \\ C_L & - & C_L(\alpha) \\ \Gamma & - & \left(\frac{1}{2} C_L V^* c \right) \\ u_a^* & - & \left([\bar{u}_a^*] \cdot [\Gamma] \right) \\ u_t^* & - & \left([\bar{u}_t^*] \cdot [\Gamma] \right) \end{bmatrix} \tag{2.3}$$

where $C_L(\alpha) \approx C_{L_e} + 2\pi(\alpha - \alpha_I)$ before stall and approximately constant post stall. Between solver iterations, $\{\beta_i, \bar{u}_a^*$, and $\bar{u}_t^*\}$ are updated. For each operating state, thrust, torque, and efficiency are easily calculated (Epps et al, 2009).

2.2 Cavitation

The *local cavitation number* is defined as

$$\sigma(r) \equiv \frac{p_{\text{atm}} + \rho g H - p_v}{\frac{1}{2}\rho (V^*(r))^2} \tag{2.4}$$

with atmospheric pressure $p_{\text{atm}} = 101$ kPa, seawater density $\rho = 1025$ kg/m^3, gravity $g = 9.81$ m/s^2, shaft centerline depth H, and vapor pressure $p_v = 2500$ Pa. The pressure coefficient (at radius r and chordwise location x) is

$$C_P(r,x) \equiv \frac{p(r,x) - (p_{\text{atm}} + \rho g H)}{\frac{1}{2}\rho (V^*(r))^2} \tag{2.5}$$

Since cavitation may occur when the pressure falls below the vapor pressure, chord must be made large enough such that the minimum pressure coefficient (i.e. maximum $-C_P$) satisfies

$$[-C_P]_{\max} \le \sigma \tag{2.6}$$

(Kerwin and Hadler, 2010).

2.3 An analytic estimate of $[-C_P]_{\max}$

In order to develop a deterministic design method that satisfies (2.6), we require an analytic estimate of $[-C_P]_{\max}$. Employing Bernoulli's equation, (2.5) can be written as

$$-C_P(x) = \left\{ \frac{q(x)}{V^*} \right\}^2 - 1 \tag{2.7}$$

where $q(x)$ is the the total fluid velocity. For a 2D hydrofoil spanning $0 \le x \le c$, linear theory (with the Lighthill leading-edge correction) gives

$$\frac{q(x)}{V^*} = \left(1 + \frac{u_t(x)}{V^*} \pm \frac{u_c(x)}{V^*} \right) \sqrt{\frac{x}{x + \frac{1}{2} r_\ell}} \pm (\alpha - \alpha_I) \sqrt{\frac{c - x}{x + \frac{1}{2} r_\ell}} \tag{2.8}$$

where u_t and u_c are the perturbation velocities due to thickness and camber effects, respectively, and r_ℓ is the leading-edge radius.

A typical propeller blade section may be generated using a NACA 'a'-series meanline and some thickness distribution. A NACA 'a'-series camber line scaled for ideal lift coefficient C_{L_I} has a camber perturbation velocity of $\frac{u_c(x)}{V^*} \approx \frac{1}{2} \frac{C_{L_I}}{(1+a)}$. The thickness perturbation velocity is proportional to the thickness ratio, $\frac{u_t(x)}{V^*} \approx a_1 \tau$, where we define $\tau \equiv \frac{t_0}{c}$. Typical values of a_1 are $\frac{4}{\pi}$, 1.20, and 1.18 for the 'parabolic', 'NACA 65A010', and 'NACA66' thickness forms, respectively. The leading edge radius is proportional to the square of the thickness ratio, $\frac{r_\ell}{c} = \rho_\ell \tau^2$, where ρ_ℓ is the leading edge radius ratio for unit thickness ratio.

Thus, for the *upper* surface (suction side)

$$-C_P(x) \approx \left\{ A_1 \sqrt{\frac{x}{x + \frac{1}{2} r_\ell}} + A_2 \sqrt{\frac{c - x}{x + \frac{1}{2} r_\ell}} \right\}^2 - 1 \tag{2.9}$$

$$A_1 \equiv 1 + a_1 \tau + \frac{1}{2} \frac{C_{L_I}}{(1+a)} \tag{2.10}$$

$$A_2 \equiv \alpha - \alpha_I \tag{2.11}$$

and for the *lower* surface (pressure side)

$$-C_P(x) \approx \left\{ A_3 \sqrt{\frac{x}{x + \frac{1}{2} r_\ell}} + A_4 \sqrt{\frac{c - x}{x + \frac{1}{2} r_\ell}} \right\}^2 - 1 \tag{2.12}$$

$$A_3 \equiv 1 + a_1 \tau - \frac{1}{2} \frac{C_{L_I}}{(1+a)} \tag{2.13}$$

$$A_4 \equiv -(\alpha - \alpha_I) \tag{2.14}$$

Case 1: small net angle of attack.

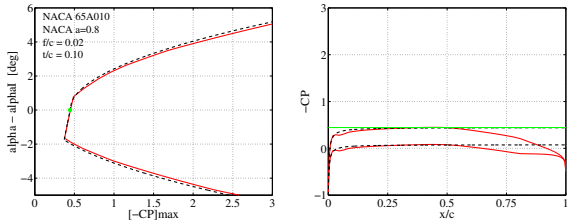

Case 2: large positive net angle of attack.

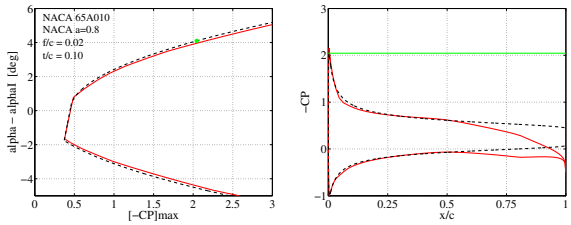

Case 3: large negative net angle of attack.

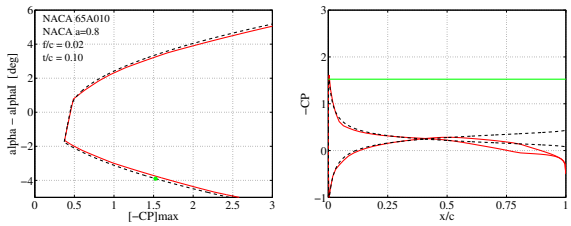

Figure 2: Brockett diagram and pressure distributions: VLM '–'; eqns. (2.9) and (2.12) '- -'; $[-C_P]_{\max}$ eqn. (2.20) '–'.

Brockett (1966) created the cavitation bucket diagram (Fig. 2), which plots $(\alpha-\alpha_I)$ versus $[-C_P]_{\max}$ for a particular camber ratio (i.e. fixed C_{L_I}) and thickness ratio ($\tau \equiv t_0/c$). These curves display three distinct regions:

Case 1: small net angle of attack (linear region). $[-C_P]_{\max}$ is located at $x/c \approx 1/2$ on the upper surface. Since $r_\ell/c \ll 1$, equation (2.9) reduces to

$$[-C_P]_{\max} \approx A_1^2 + 2A_1A_2 - 1 \tag{2.15}$$

which is indeed linearly-proportional to $(\alpha-\alpha_I)$.

Case 2: large positive net angle of attack (non-linear region). Setting, $\frac{d}{dx}([-C_P]_{\max}) = 0$ in (2.9) gives the location of $[-C_P]_{\max}$ on the upper surface

$$x/c = \frac{A_1^2}{A_1^2 + A_2^2(1+2c/r_\ell)^2} \tag{2.16}$$

Inserting (2.16) into (2.9) yields

$$[-C_P]_{\max} \approx A_1^2 + A_2^2(2c/r_\ell) - 1 \tag{2.17}$$

Comparing (2.15) and (2.17), case 2 is when $A_2 > A_1\, r_\ell/c$.

Case 3: large negative net angle of attack (non-linear region). Here, $[-C_P]_{\max}$ is located on the lower surface at

$$x/c = \frac{A_3^2}{A_3^2 + A_4^2(1+2c/r_\ell)^2} \tag{2.18}$$

(A_3 and A_4 are both positive) and similar to case 2,

$$[-C_P]_{\max} \approx A_3^2 + A_4^2(2c/r_\ell) - 1 \tag{2.19}$$

This is the case when, by quadratic formula, $A_4 > (-2A_1 + \sqrt{(2A_1)^2 - 4(2c/r_\ell)(A_3^2 - A_1^2)})/(2\cdot(2c/r_\ell))$.

Thus, the bucket diagram can be formed as follows

$$[-C_P]_{\max} \approx \begin{cases} A_1^2 + 2A_1A_2 - 1 & \text{(case 1)} \\ A_1^2 + A_2^2(2c/r_\ell) - 1 & \text{(case 2)} \\ A_3^2 + A_4^2(2c/r_\ell) - 1 & \text{(case 3)} \end{cases} \tag{2.20}$$

The bucket diagram can also be computed numerically, given the 2D geometry. The VLM code employed herein (Kerwin, 2007), represents the blade using point sources and vortices distributed along the chord line, and the Lighthill leading edge correction is employed as well (Lighthill, 1951). Fig. 3 shows good agreement between $[-C_P]_{\max}$ computed by VLM and by (2.20) for a wide range of thickness ratios.

Equation (2.20) can be rearranged in terms of the blade loading (Γ, V^*) and the geometry (c, τ) as follows. Since camber is fixed at the (endurance speed) design point, $C_{L_I} = C_{L_e} = \frac{2\Gamma_e}{V_e^* c}$. Also, one can approximate the lift coefficient at an off-design point by $C_L = C_{L_I} + 2\pi(\alpha - \alpha_I)$. Thus, define

$$a_1 \equiv 1.20 \text{ for 'NACA 65A010'} \tag{2.21}$$

$$a_2 \equiv \frac{\Gamma_e}{V_e^*(1+a)} \tag{2.22}$$

$$a_3 \equiv \frac{1}{2\pi}\left(\frac{2\Gamma_m}{V_m^*} - \frac{2\Gamma_e}{V_e^*}\right) \tag{2.23}$$

such that

$$[-C_P]_{\max} \approx \begin{cases} \left(1 + a_1\tau + \dfrac{a_2}{c}\right)^2 + 2\left(1 + a_1\tau + \dfrac{a_2}{c}\right)\dfrac{a_3}{c} - 1 \\ \left(1 + a_1\tau + \dfrac{a_2}{c}\right)^2 + \dfrac{a_3^2}{c^2\tau^2}\dfrac{2}{\rho_\ell} - 1 \\ \left(1 + a_1\tau - \dfrac{a_2}{c}\right)^2 + \dfrac{a_3^2}{c^2\tau^2}\dfrac{2}{\rho_\ell} - 1 \end{cases} \tag{2.24}$$

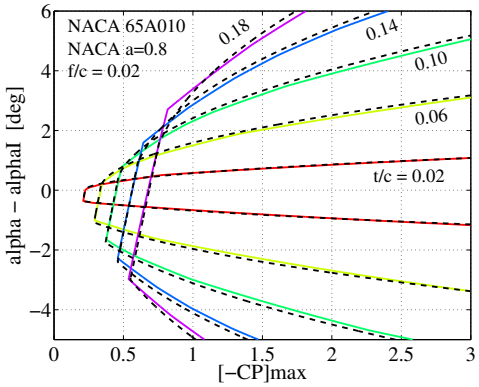

Figure 3: Brockett diagram: VLM '–'; equation (2.20) '- -'.

3.0 DESIGN OPTIMIZATION METHODS

Herein, we consider the optimization of circulation, camber, and thickness for given propeller design parameters. In the standard approach (fig. 4a), only the *endurance speed* is considered. The circulation and chord optimization procedures are performed sequentially, iterating until circulation converges (which, practically-speaking, implies that chord has converged as well). In this procedure, the chord lengths can be set to prevent cavitation at the endurance speed, but this does not ensure that cavitation is prevented at the ship's *maximum speed*. Also, this method does not typically involve blade thickness optimization.

In the present design method (Fig. 4b), both the *endurance speed* and *maximum speed* are considered automatically. An inner loop runs to optimize the circulation distribution at the *endurance speed*, and an outer loop runs to optimize the chord and thickness to prevent cavitation at the *maximum speed*. When both the circulation and chord have converged, the blade design is complete, and no further modifications are necessary.

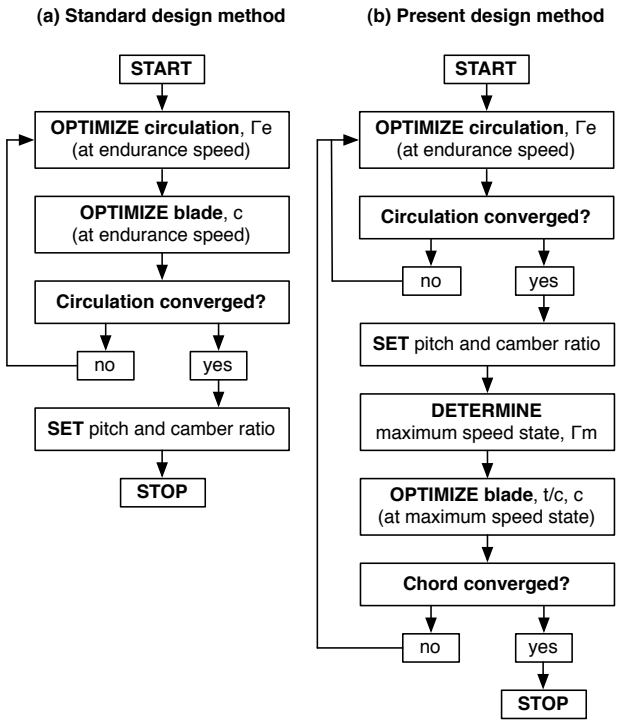

Figure 4: Propeller design optimization methods.

3.1 Circulation optimization

Circulation optimization is performed following the procedure of Kerwin, Coney, and Hsin (1986), which is to find the set of M vortex panel circulations that produce the least torque for a specified (endurance speed) thrust, $T = T_e$. They form an auxiliary function, $H = Q + \lambda_1(T - T_e)$, where λ_1 is a Lagrange multiplier, and they find the optimum Γ by setting the partial derivatives of H to zero

$$\frac{\partial H}{\partial \Gamma_{(i)}} = 0, \quad \frac{\partial H}{\partial \lambda_1} = 0 \tag{3.1}$$

which is a system of $M+1$ equations for as many unknowns $\{\Gamma_{(i=1\ldots M)}, \lambda_1\}$. For a given chord distribution, $c(r)$, this non-linear system of equations can be solved iteratively.

3.2 Off-design analysis

In the procedure outlined in Fig. 4b, we are given a *maximum ship speed*, V_m, and required thrust, T_m, and we now need to determine the required rotation speed, ω_m so we can use the procedure in §2.1 to determine the max-speed loading $\{\Gamma_m,\ V_m^*,\ \text{etc.}\}$, which is required for blade shape optimization. From the given information, we can formulate the required thrust coefficient (C_{T_m} or K_{T_m})

$$C_{T_m} = \frac{T_m}{\frac{1}{2}\rho V_m^2 \pi R^2} = \frac{8}{\pi}\frac{K_{T_m}}{J_m^2} \tag{3.2}$$

We now present a fast algorithm to determine the required advance coefficient $J_m = \frac{\pi V_m}{\omega_m R}$, such that $C_T(J_m) = C_{T_m}$.

First note that for most propellers, the $K_T(J)$ curve is nearly linear.

$$K_{T_m} \equiv K_T(J_m) \approx K_T(J) + K_T'(J)\cdot(J_m - J) \tag{3.3}$$

where $K_T' \equiv \frac{dK_T}{dJ}$ can be estimated using finite differences between two prior $K_T(J)$ values. Thus,

$$C_{T_m} \approx \frac{8}{\pi}\frac{K_T(J) + K_T'(J)\cdot(J_m - J)}{J_m^2} \tag{3.4}$$

Given current J, $K_T(J)$, and $K_T'(J)$ values, the next guess for J_m is then

$$J_m \approx \frac{K_T' + \sqrt{(K_T')^2 - 4(\frac{\pi}{8}C_{T_m})(K_T'\cdot J - K_T)}}{2(\frac{\pi}{8}C_{T_m})} \tag{3.5}$$

This typically only takes a few iterations to converge on the J_m needed such that $C_T(J_m) = C_{T_m}$.

3.3 Chord length optimization

Three chord length optimization methods are now presented. Methods 1 and 2 must be used with procedure (Fig. 4a), while method 3 is used with (Fig. 4b). A cavitation margin, μ, can be implemented in methods 2 and 3 by replacing σ with $\mu\sigma$ in the following equations.

3.3.1 *Method 1: maximum lift coefficient*

Since lift coefficient is related to the pressure difference across the blade section, it is a proxy measure of cavitation performance. Typically, to mitigate cavitation inception (particularly at the root and tip) section lift coefficients are limited to a maximum allowable distribution:

$$C_{L_{\max}}(r) = 0.5 + (0.2 - 0.5)\frac{r - R_{\text{hub}}}{R_{\text{tip}} - R_{\text{hub}}} \tag{3.6}$$

which yields 0.5 at the hub and 0.2 at the tip. Thus, the optimum chord length is

$$c = \frac{2\,\Gamma_e}{V_e^* C_{L_{\max}}} \tag{3.7}$$

While this simple method ensures adequate loading at the (endurance speed) design point, it does not necessarily prevent cavitation, nor does it prescribe the optimum thickness distribution.

3.3.2 *Method 2: Brockett diagram map*

Coney (1989) sets the chord distribution based on the following equation:

$$\sigma(r) = 26.67\frac{f_0^2}{c^2} + 8.09\frac{f_0}{c} + 10.0\frac{f_0}{c}\frac{t_0}{c} + 3.033\frac{t_0}{c} \tag{3.8}$$

which approximately sets $[-C_P]_{\max} = \sigma$ at the transition between case 1 and case 2 of the Brockett bucket diagram; thus, it provides the optimum angle of attack envelope for the given thickness, camber (2.1), and cavitation number (2.4).

This method can only be used to optimize the chord distribution at the *endurance speed*, as equation (2.1) sets the blade camber for the required loading at this design point, and equation (3.8) implicitly assumes that the angle of attack of the blade section is the ideal angle of attack, to center the blade section in its Brockett bucket curve. This method also requires $t_0(r)$ to be specified.

3.3.3 *Method 3: linear foil theory C_P*

Using equation (2.24) to estimate $[-C_P]_{\max}$, we are now equipped to optimize both c and τ to prevent cavitation at the *maximum speed*, for which we have computed Γ_m, V_m^*. Since $T_m > T_e$, $\alpha - \alpha_I > 0$, and either case 1 or case 2 will apply.

Contours of $[-C_P]_{\max}$ for case 1 and case 2 are shown in Fig. 5, with $[-C_P]_{\max} = \sigma$ highlighted in red. It is clear that for case 2, when

$$\left(1 + a_1\tau + \frac{a_2}{c}\right)^2 + \frac{a_3^2}{c^2\tau^2}\frac{2}{\rho_\ell} - 1 = \sigma \tag{3.9}$$

there is an optimum τ that minimizes c. Thus, a second constraint equation is that $\frac{dc}{d\tau} = 0$ while traversing the contour defined by (3.9):

$$2a_1\left(1 + a_1\tau + \frac{a_2}{c}\right) - 2\frac{a_3^2}{c^2\tau^3}\frac{2}{\rho_\ell} = 0 \tag{3.10}$$

Equations (3.9) and (3.10) form a deterministic set of equations that prescribe (c, τ) given $(\Gamma_e, V_e^*, \Gamma_m, V_m^*$, and $\sigma)$.

For case 1,

$$\left(1 + a_1\tau + \frac{a_2}{c}\right)^2 + 2\left(1 + a_1\tau + \frac{a_2}{c}\right)\frac{a_3}{c} - 1 = \sigma \tag{3.11}$$

As shown in Fig. 5, setting $\tau = 0$ minimizes the chord length, but this is not possible due to strength considerations. If the τ from case 2 is selected, then (3.11) yields the optimum chord. The larger of the chord lengths required by case 1 and case 2 is then selected.

Surprisingly, this procedure naturally results in $\tau(r)$ that varies nearly linearly along the span of the blade. The required chord length at the root is quite short, and the blade is quite thin at the root, which is not a practical design solution. In particular, the resulting blade does not meet the American Bureau of Shipping (ABS) standards for blade thickness at the root. Thus, an additional modification to the blade shape is required.

Case 1: small net angle of attack.

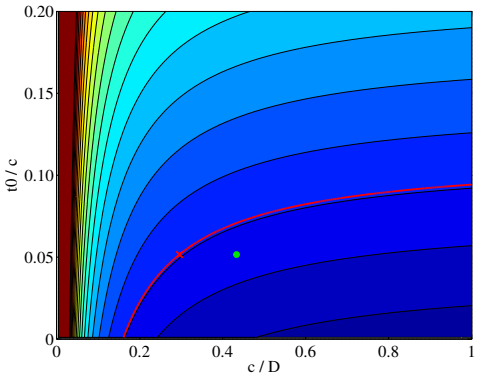

Case 2: large positive net angle of attack.

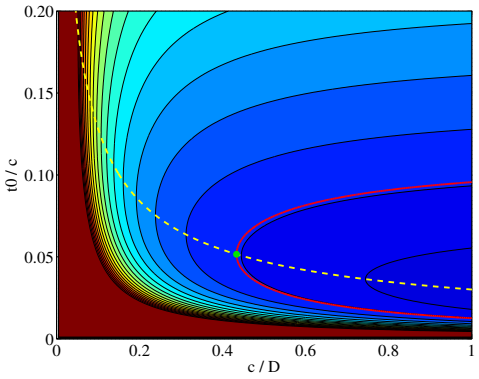

Figure 5: Contours of $[-C_P]_{\max}$, with $[-C_P]_{\max} = \sigma$ in red, optimum $(t_0/c, c)$ '•', and equation (3.10) '- - '.

3.3.4 ABS thickness requirement

The American Bureau of Shipping standard requires minimum blade thickness to meet strength requirements (ABS, 2007). The formula is quite complex but can be simplified as follows:

$$\frac{t_{0_{25}}}{D}\sqrt{\frac{c_{25}}{D}} \approx T_1 \tag{3.12}$$

where

$$T_1 \equiv \frac{T_0}{10^6}\sqrt{\frac{1+6/p_{70}+4.3p_{25}}{1+1.5p_{25}}\frac{\mathcal{P}}{fND^3\mathcal{Z}}}$$

$T_0 \equiv 1.025\cdot 337/\sqrt{0.1}$ in SI units, p is pitch to diameter ratio, D is diameter [m], $f \equiv 2.62$ for nickel-aluminum bronze, N is RPM at endurance speed, $\mathcal{P}$ is power at endurance speed [W], $\mathcal{Z}$ is number of blades, and the subscripts 25 and 70 indicate $r/R = 0.25$ and 0.75, respectively.

For a given thickness ratio distribution (namely, t_0/c at $r = 0.25R$), equation (3.12) can be used to find the required thickness at the 0.25 radius

$$\frac{t_{0_{25}}}{D} \approx \left(T_1\sqrt{(t_0/c)_{25}}\right)^{2/3} \tag{3.13}$$

To meet this requirement, the thickness distribution is modified as shown in Fig. 6. The new thickness distribution is linear from $r/R = 0.25$ to the point where it intersects the old thickness distribution tangentially and then follows the old thickness distribution out to the tip. While holding t_0/c constant, chord is increased to meet this new thickness distribution.

$$\left(\frac{c}{D}\right)_{\text{new}} = \frac{(t_0/D)_{\text{ABS}}}{(t_0/c)_{\text{old}}} \tag{3.14}$$

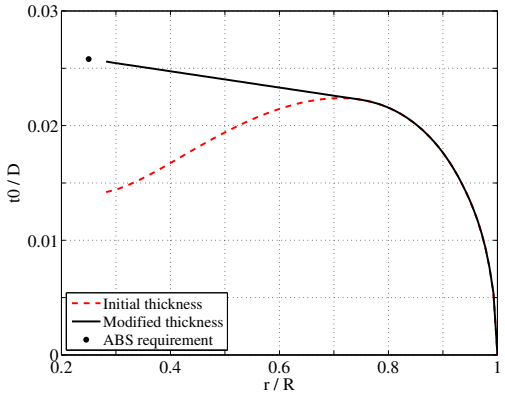

Figure 6: Thickness modification to meet (3.12).

4.0 ILLUSTRATIVE EXAMPLE

An illustrative example is presented that combines the performance specifications for the DDG51 destroyer-class vessel (Tsai et al, 1994) with those of David Taylor Propeller 5168 (Chesnakas and Jessup, 1998). DTMB 5168 is a representative modern surface ship controllable-pitch propeller. The primary design parameters are listed in Table 1. Where possible, the design parameters follow those of propeller 5168, namely $\mathcal{Z}$, D, and D_{hub}/D. The thrust requirements at the $V_e = 20$ knot *endurance speed* and $V_m =$ 30 knot *maximum speed* were formed by multiplying the values in (Tsai et al, 1994) by 1.09, in order to match the K_T requirement at the endurance speed with that of propeller 5168. The rotation rate at endurance speed was then chosen to match the advance ratio of propeller 5168.

The inflow velocity profile was assumed uniform ($V_a/V_s = 1$ and $V_t/V_s = 0$ for all blade sections). Although propeller 5168 employs rake and skew, these were set to zero for this study. The section drag coefficient was assumed to be $C_D = 0.008$ for all blade sections. Blade sections were formed using the 'NACA a=0.8' meanline and 'NACA 65A010' thickness forms.

Four propellers were designed in this study, as summarized in Table 2. The 'Epps w/ ABS' propeller employs the present design methods detailed in Fig. 4b, §3.3.3, and §3.3.4. To highlight the effect of the ABS requirement, the 'Epps w/o ABS' propeller was designed using only Fig. 4b and §3.3.3. The standard design method (Fig. 4a) yields the 'CLmax' propeller (§3.3.1) or the 'Coney' propeller (§3.3.2). The 'CLmax' and 'Coney' propellers used the thickness distribution (t_0/D) from the 'Epps w/ ABS' design.

Table 1: Propeller design input parameters.

Parameter	Description
$\mathcal{Z} = 5$	number of blades
$D = 5.18$ m	diameter (17 ft)
$D_{\text{hub}} = 1.46$ m	hub diameter ($0.2819D$)
$N_e = 93.8$ RPM	rotation rate at V_e
$V_e = 10.29$ m/s	endurance speed (20 kts)
$T_e = 4.159$e5 N	thrust at V_e
$V_m = 15.43$ m/s	max speed (30 kts)
$T_m = 1.38$e6 N	thrust at V_m
$\rho = 1025$ kg/m^3	sea-water density
$H = 6.31$ m	shaft depth (20.7 ft, at draft)
$M = 20$	number of vortex panels

Table 2: Summary of design methods.

Name	Design methods
'Epps w/ ABS'	Fig. 4b, §3.3.3, §3.3.4
'Epps w/o ABS'	Fig. 4b, §3.3.3
'CLmax'	Fig. 4a, §3.3.1
'Coney'	Fig. 4a, §3.3.2

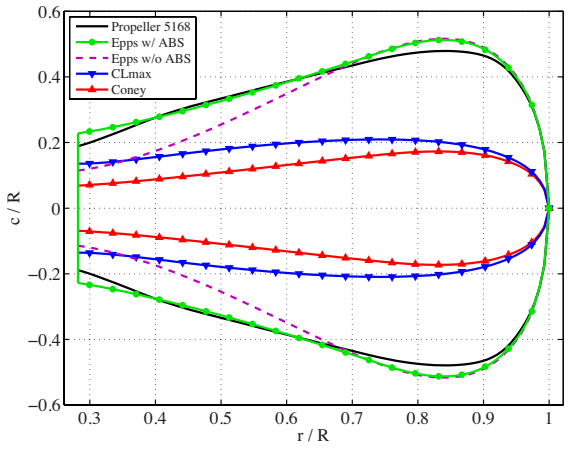

Figure 7: Chord distribution.

The blade outline for the four propellers and propeller 5168 are shown in Fig. 7. The 'Epps w/ ABS' design well replicates Navy propeller 5168, which validates that the procedures in §3.3.3 and §3.3.4 yield a realistic blade outline. The 'Epps w/o ABS' propeller has a similar tip but much shorter chord lengths (and thicknesses, as shown in Fig. 8d) near the root. This illustrates how the ABS thickness requirement augments the required blade shape. Both the 'CLmax' and 'Coney' propellers have much shorter chord lengths, as these are only designed to mitigate cavitation at the endurance speed.

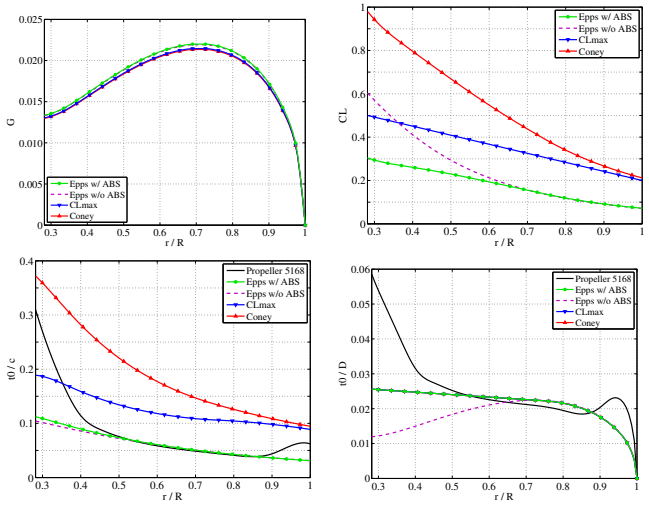

Figure 8: Performance of the four propeller designs, where $G = \frac{\Gamma_e}{2\pi R V_e}$ and $C_L = \frac{2\Gamma_e}{(V_e^*)c}$.

Fig. 8 shows additional comparisons between these four propeller designs. Fig. 8a shows that the endurance speed circulation loading is nearly identical for the four designs; this is because viscous parasitic drag forces are small ($F_v = \frac{1}{2}\rho(V^*)^2 C_D c$, with $C_D = 0.008$), so nearly the same circulation loading is required regardless of the chord lengths. Fig. 8b shows lift coefficient. Interestingly, the 'Epps w/ ABS' procedure results in a nearly linear C_L distribution over the span of the blade. In this case, these lift coefficients are about half of those that we arbitrarily chose for the 'CLmax' propeller. This shows that while the 'CLmax' procedure (§3.3.1) is sound, it doesn't necessarily mitigate cavitation. Figs. 8c and 8d show the thickness ratio and thickness, respectively. Note that the 'Epps w/ ABS' propeller has nearly the same thickness distribution as P5168, providing another validation for this method. The 'Epps w/o ABS' has a slightly different t_0/c as the 'Epps w/ ABS'; although t_0/c is fixed in the ABS procedure (§3.3.4) during each optimizer iteration, the optimizer converged on slightly different results after multiple iterations. Since the 'CLmax' and 'Coney' propellers used the t_0/D from the 'Epps w/ ABS' design but have smaller chord lengths, the t_0/c distributions are much larger and are in fact impractical. This emphasizes the advantage o the present procedure, which optimizes both thickness and chord with no *a priori* assumptions.

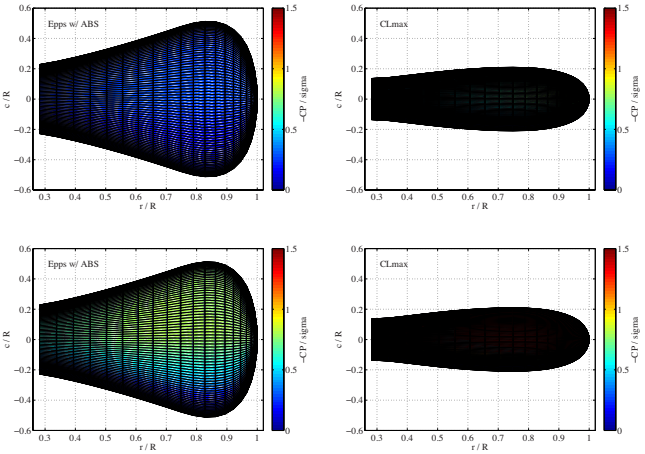

Figure 9: Suction-side pressure distribution shows cavitation performance: (top) endurance speed, (bottom) maximum speed.

Fig. 9 compares the suction-side cavitation performance of the 'Epps w/ ABS' propeller to the 'CLmax' propeller. The pressure distributions were computed here using the 2D VLM solver applied to each blade section. The top panel shows that both are cavitation free at the endurance speed. The lower panel shows that while the 'Epps w/ ABS' propeller is still cavitation free at the maximum speed – as expected – the 'CLmax' propeller shows significant suction-side cavitation.

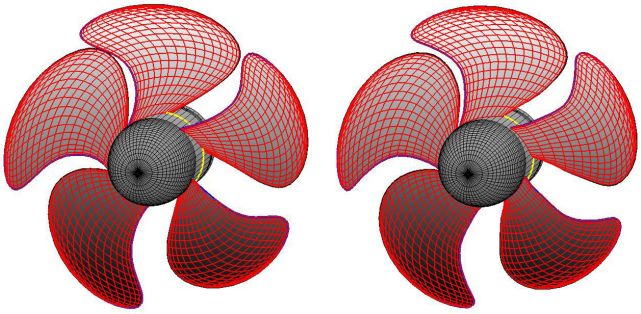

Figure 10: Design 'Epps w/ ABS' (left) versus Propeller 5168 (right).

Finally, Fig. 10 compares the 3D geometry of P5168 to the 'Epps w/ ABS' propeller. For comparison, the rake and skew distribution of P5168 were used for both figures. These figures show that the 'Epps w/ ABS' procedure (Fig. 4b, §3.3.3, and §3.3.4) clearly yields a realistic and representative propeller blade design.

5.0 CONCLUSION

This paper presents an analytic estimate of the minimum pressure coefficient on a 2D non-cavitating hydrofoil (2.20). This estimate was used to develop an analytic approximation to the cavitation bucket diagrams typically used in marine propeller design. Further, a novel design procedure was developed to optimize blade loading for maximum efficiency at an endurance speed while mitigating cavitation at a maximum speed (Fig. 4b). To enable this procedure, a method was developed to efficiently find the advance coefficient needed to produce a required thrust coefficient (§3.2). Using the analytic estimate of the minimum pressure coefficient, it was found that an optimum chord length and thickness ratio exist, such that chord is minimized while the negative pressure coefficient does not exceed the cavitation number (§3.3.3). Finally, we illustrated this novel optimization procedure in application the DDG51 destroyer-class vessel (§4.0). The present methods are coded in the OPENPROP suite (Kimball and Epps, 2010) and are readily-available for academic and industrial use. This work extends the capabilities of OPENPROP to high-speed ship propulsion applications.

The design optimization procedure developed herein is an automated, deterministic design approach, which enables parametric studies comparing various design inputs, such as propeller diameter, endurance speed rotation rate, and number of blades.

REFERENCES

Abbott, I.H. and von Doenhoff, A.E. (1959) Theory of Wing Sections. Dover.

ABS (2007) Rules for Building and Classing Steel Vessels. American Bureau of Shipping.

Brockett, T.E. (1966) "Minimum Pressure Envelopes for Modified NACA-66 Sections with NACA a=0.8 Camber and Buships Type I and Type II Sections". DTMB Report 1780, Carderock, MD.

Chesnakas, C. and Jessup, S. (1998) "Cavitation and 3-D LDV Tip-Flowfield Measurements of Propeller 5168". Tech. rep., Naval Surface Warfare Center, Carderock, MD.

Coney, W.B. (1989) A Method for the Design of a Class of Optimum Marine Propulsors. PhD thesis, MIT, Cambridge, MA.

Epps, B.P. (2010a) An Impulse Framework for Hydrodynamic Force Analysis: Fish Propulsion, Water Entry of Spheres, and Marine Propellers. PhD thesis, MIT, Cambridge, MA.

Epps B (2010b) "OPENPROP v2.4 Theory Document". Tech. rep., MIT, http://openprop.mit.edu.

Epps, B.P.; Chalfant, J.S.; Kimball, R.W.; Techet, A.H.; Flood, K.; Chryssostomidis, C. (2009) "OPENPROP: An Open-Source Parametric Design and Analysis Tool for Propellers". Proc. Grand Challenges in Modeling and Simulation, Istanbul, Turkey.

Kerwin, J.E. (2007) Hydrofoils and Propellers. MIT Course 2.23 notes.

Kerwin, J.E. and Hadler, J.B. (2010) Principles of Naval Architecture: Propulsion. SNAME.

Kerwin, J.E.; Coney, W.B.; Hsin, C.Y. (1986) "Optimum Circulation Distributions for Single and Multi-Component Propulsors." Twenty-First American Towing Tank Conference, p. 53 – 62.

Kimball, R.W. and Epps, B.P. (2010) OPENPROP code suite. Open-source at http://openprop.mit.edu.

Lerbs, H.W. (1952) "Moderately Loaded Propellers with a Finite Number of Blades and an Arbitrary Distribution of Circulation". SNAME Transactions. vol. 60.

Lighthill, M.J. (1951) "A New Approach to Thin Aerofoil Theory". The Aeronautical Quarterly **3**(2):193–210.

Tsai, S.J.; Hopkins, B.; Stenson, R. (1994) "Comparison of Powering Performance Between DDG-51 and Conventional Combatant Hull Forms". Naval Engineers Journal **106**(5):88–99.

ACKNOWLEDGEMENTS

This work is supported by the Office of Naval Research N00014-11-1-0598, and the MIT Sea Grant College Program, NA060AR4170019 and NA10OAR4170086. In addition, the authors wish to thank Mr. Robert Damus of Project Ocean, who was instrumental in securing funds that made some of this research possible.